Fatigue crack growth rate and fractography of Ti6Al4V(ELI) specimens produced through direct metal laser sintering

Lehlohonolo Francis Monaheng[1*], *Willie Bouwer* du Preez[2], and *Claudia* Polese[3&4]

[1]Department of Mechanical and Mechatronics Engineering, Faculty of Engineering, Built Environment and Information Technology, Central University of Technology, Free State, Bloemfontein 9300, South Africa
[2]Centre for Rapid Prototyping and Manufacturing, Faculty of Engineering, Built Environment and Information Technology, Central University of Technology, Free State, Bloemfontein 9300, South Africa
[3]School of Mechanical, Industrial and Aeronautical Engineering, University of the Witwatersrand, Johannesburg 2050, South Africa
[4]ARUA Centre of Excellence in Materials, Energy and Nanotechnology, University of the Witwatersrand, Johannesburg 2050, South Africa

Abstract. Fractographic analysis was conducted on Ti6Al4V(ELI) fatigue crack growth rate (FCGR) specimens produced via direct metal laser sintering (DMLS) to determine their failure mechanism and to generate data required for qualification of DMLS as a manufacturing technology for aircraft structural components. The specimens were built in three orientations and subsequently subjected to a two-stage heat treatment. All specimens were then tested in compliance with the ASTM E647-23a standard for FCGR measurement. Scanning electron microscopy (SEM) was used to examine the fracture surfaces and identify the underlying failure mechanisms. The observed fracture surfaces exhibited tortuous features with fibrous and lamellar tearing, characteristic of strong metallurgical bonding between the DMLS layers. The findings confirm that Ti6Al4V(ELI) aircraft components can indeed be successfully manufactured using DMLS.

1 Introduction

Fatigue and tensile strength are among the most critical material parameters when designing aircraft components that must endure cyclic loading throughout their service life [1]. Ti6Al4V(ELI) (extra low interstitials) is an $(\alpha + \beta)$ titanium alloy commonly used for its unique combination of low density, good corrosion resistance, excellent mechanical properties and fatigue crack growth (FCG) resistance [2]. The good fatigue and mechanical properties of the Ti6Al4V(ELI) alloy attract the use of laser powder bed fusion (LPBF) technology to produce complex-shaped aircraft components. DMLS, which is categorised

* Corresponding author: lmonaheng@cut.ac.za

under LPBF, is a layer-by-layer powder deposition technique that fuses layers of metal powder to create three-dimensional (3D) objects from digital computer model data, resulting in minimal material wastage, with the added benefit that un-melted powder can be reused [3]. However, the DMLS process can induce unwanted residual stress due to rapid solidification that results from high thermal gradients that occur during the fusion process.

The as-built DMLS Ti6Al4V(ELI) specimens were reported to have acicular α'grains and higher tensile strength and Young's modulus than parts produced through traditional manufacturing processes, such as casting and forging, but had low elongation ranging between 2 and 6% [4]. To relieve detrimental residual stress DMLS Ti6Al4V(ELI) specimens are normally submitted to a heat treatment at a temperature of 650℃ for a period of 3 hours [5]. Subsequent to stress relieving, a high temperature annealing heat treatment is commonly applied at a temperature that is very close to or slightly above the β-transus temperature resulting in a microstructure with a mixture of $\alpha + \beta$ phase [6]. This microstructure is associated with higher fatigue properties as compared to the wrought alloy [7]. Therefore, the fatigue and static mechanical properties of Ti6Al4V(ELI) parts produced through DMLS can be optimised by altering their microstructure through high temperature annealing.

A complex shaped structure of an aircraft, such as a nose wheel fork, resulting from topology optimisation design for additive manufacturing (DfAM), can be produced through DMLS [8]. Furthermore, the DMLS technology has various benefits over the conventional manufacturing method. These include reduction of the production cost of a complex component, high level of design freedom and rapid prototyping [9]. However, at this stage, the requirement of the aviation industry for a qualified manufacturing method limits the use of DMLS for the production of aircraft components from the Ti6Al4V(ELI) alloy, particularly for mission-critical applications [10][11].

The fatigue properties of Ti6Al4V(ELI) components produced through DMLS are affected by various factors such as lack-of-fusion, residual stress, microstructure and surface roughness. When the alloy fails to melt or fuse completely, lack-of-fusion defects can form at localised regions in the DMLS Ti6Al4V(ELI) component [12]. These defects and pores can induce cracking of the DMLS Ti6Al4V(ELI) components thereby compromising the fatigue life. Finally, Ti6Al4V(ELI) structural components of an aircraft produced through DMLS exhibit relatively high surface roughness, which acts as stress concentrator and is sufficient to initiate cracks [13].

Qualification challenges of selective laser melting (SLM) for application in aerospace to produce aircraft components were discussed by Dordlofva et al. [14]. Stringent standards in the aircraft industry must be complied with to qualify LPBF as a manufacturing method for the production of aircraft parts [10]. Portolés et al. [15] proposed a qualification procedure to reproduce and repair metal aerospace components through electron beam melting. Generally, there is consensus that the qualification and certification process of LPBF for application in aerospace should not differ from that of the conventional manufacturing process [16].

Authorities, such as the Federal Aviation Administration (FAA) and the European Aviation Safety Agency (EASA), provide regulations and standards for the approval of aircraft parts and certify every technology used for the production of such parts [10]. Locally, the South African Civil Aviation Authority (SACAA) ensures safety and security in support of the sustainable development of the aviation industry. For example, FAA 23.627 [17] is the relevant regulation for determining the fatigue strength of structural aircraft parts, whereas SACAA provides the technical guidance for approval of manufactured parts [18].

The capability of an aircraft component to withstand repeated loads of variable magnitude, as expected in service, must be demonstrated through classical analysis or

standard experimental test methods [17][19]. The ASTM E647-23a standard is the recognised method for determining the fatigue crack growth rate (FCGR) of parts [20].

A crucial requirement for the qualification of a Ti6Al4V(ELI) component produced through LPBF is the characterisation of the fracture mechanisms in accordance with recognised testing standards [21]. Fracture surface analysis provides reliable robust evidence to validate key material properties, including ductility, fracture toughness and fatigue crack growth rate FCGR [22]. For DMLS-produced Ti6Al4V(ELI) components, fracture modes are influenced by build process parameters, build orientation and post-process heat treatments. Consequently, multiple experimental datasets are required to complete the full qualification process.

In this study, the FCGR testing and fractography analysis were performed on DMLS Ti6Al4V(ELI) specimens subjected to a two-stage heat treatment, to determine their failure mechanism and generate data necessary to support the qualification of DMLS as a viable manufacturing technology for aircraft structural components. This study was motivated by the South African Additive Manufacturing Strategy, which prioritises the qualification of AM parts for the aerospace industry [23].

2 Material and methods

Tensile specimens were tested in compliance with the ASTM E8/E8M standard method [24] to verify the quality of the DMLS build process. The microstructure of the Ti6Al4V(ELI) specimens built through DMLS was the examined using optical microscopy. Subsequently, fatigue crack growth rate FCGR testing was carried out following ASTM E647 standards [25]. The results were compared with data from alternative heat treatment processes reported in literature. Finally, fracture surface characteristics were analysed using scanning electron microscopy (SEM).

2.1 Preparation of specimens

Spherical Ti6Al4V(ELI) powder supplied by TLS Technik (TLS Technik GmbH & Co Spezialpulver KG, Bitterfeld-Wolfen, Germany) was used to build the tensile and FCGR compact test (CT) specimens. This powder had an average particle size of less than 45 μm and a chemical composition that complied with ASTM F3001-14 [26], as shown in Table 1.

Table 1. Chemical composition of TLS Technik Ti6Al4V(ELI) powder and the ASTM F3001 specification.

Specification	Titanium (Ti)	Aluminium (Al)	Vanadium (V)	Iron (Fe), max	Oxygen (O), max	Nitrogen (N), max
TLS powder	90.30%	5.56%	4.02%	0.23%	0.12%	0.04%
ASTM F3001-14 [26]	Balance	5.5–6.5%	3.5–4.5%	0.25%	0.13%	0.05%

An EOSINT M280 SLM machine (EOS GmbH, Munich, Germany), equipped with a 200 W ytterbium fibre laser with a laser beam diameter of 80 μm, and powder layer thickness of 30 μm, was used to build all specimens. A total of nine FCGR specimens were produced following the ASTM E647-23a standard [25], three in each of the XZY-, YXZ-, and ZXY-orientations, as shown in Figure 1. These specimens were prepared following the ASTM E647-23a standard [25]. To verify the build process, triplicate cylindrical tensile test specimens were manufactured along each of the X-, Y-, and Z-axis orientations following

ASTM E8 [24]. These tensile specimens were produced in a standard cylindrical geometry without surface finishing, thereby retaining the as-built surface roughness.

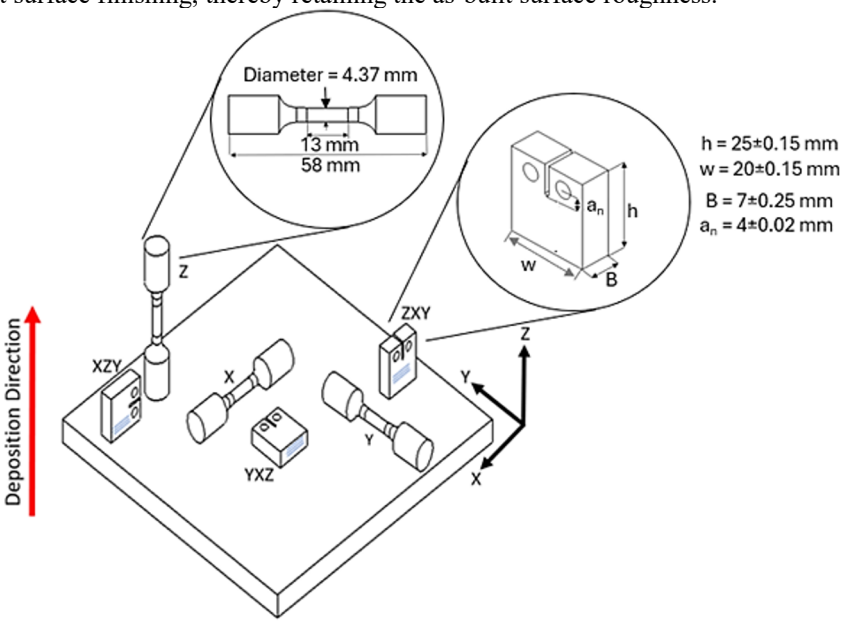

Fig. 1. Illustration of the building orientations of the cylindrical tensile test specimens and FCGR compact test specimens.

All specimens underwent a two-stage heat treatment previously proposed for Ti6Al4V(ELI) aircraft components manufactured through selective laser melting (SLM) [27]. The improvement in the fatigue strength of DMLS Ti6Al4V(ELI) specimens reported in previous studies [28][29] served as the primary motivation for selecting the heat treatment used in this work.

Firstly, while still secured to the base plate, the specimens were heated at a rate of 3.6 °C/min in a vacuum furnace to 650 °C and soaked at this temperature for 3 hours before being furnace-cooled to room temperature. The specimens were then cut off the base plate using a wire electrical discharge machine, followed by manual removal of the support structures. Because there were support structures between the specimens and the baseplate, the cutting did not penetrate the specimens. Therefore, the electric discharge machining had no negative impact on the specimens. Subsequently, the test specimens were heated to 950 °C at a rate of 5.2 °C/min in a vacuum furnace and soaked at 950 °C for 2 hours before being furnace-cooled to room temperature. This was done to obtain a microstructure consisting of a mixture of acicular α-phase plus β-phase.

The microstructures of the specimens were studied using a ZEISS Axio Observer optical microscope (Zeiss, Oberkochen, Germany). For the specimens built in the XZY-, YXZ- and ZXY-orientations, the microstructures in the XY-, ZX- and ZY-planes were evaluated (see coordinate system shown in Figure 1). Firstly, samples were prepared using 46 µm waterproof SiC grinding discs. Thereafter, samples were mechanically polished on a Struers Tegramin-25 machine (Struers LLC, Cleveland, OH, US), using DiaMaxx Poly 9 and 3 μm diamond suspensions. To complete the metallographic preparation, etching was done on all samples using Kroll's reagent.

2.2 Analysis of fatigue crack growth rate

Fracture mechanics parameters, such as the stress-intensity factor and crack size, are used to correlate the rate of cracking [30]. For instance, the FCGR $\left(\frac{da}{dN}\right)$ of an alloy, such as Ti6Al4V(ELI), can be described by the Paris law given in Equation 1:

$$\frac{da}{dN} = C(\Delta K)^m \quad (1)$$

where C and m, obtained experimentally, are material, environment, frequency, temperature and stress ratio-dependent constant values. ΔK, a and N are the stress-intensity range, crack length and the number of cycles to failure, respectively. Importantly, ΔK is directly dependent on the crack length a, the cyclic stress range σ_r and the geometry correction factor Y, as expressed in Equation 2.

$$\Delta K = Y\sigma_r\sqrt{\pi a} \quad (2)$$

Commonly, the FCGR is plotted against ΔK using a logarithmic scale to illustrate three distinct regions of FCGR behaviour, which are slow crack growth, power-law behaviour (Paris' region) and rapid unstable crack growth. Therefore, Equation 1 can be modified as shown by Equation 3. It is clear from Equation 3 that m is the slope of the logarithmic FCGR versus ΔK plot and C is the intersect value.

$$log\left(\frac{da}{dN}\right) = m \cdot log\Delta K + logC \quad (3)$$

2.3 Mechanical testing procedure

The tensile testing of the Ti6Al4V(ELI) specimens was performed according to ASTM E8 using a 30 kN Instron 1342 servo-hydraulic testing machine (Instron, Norwood, US). The same machine was used for FCGR tests following ASTM E647. In Table 2, the pre-crack termination values and FCGR testing conditions are stated. The test was performed through constant load amplitude control. For this, machine controlled the applied load amplitude to the specimen, maintaining P_{min}/P_{max} of 0.1. Therefore, FCGR was increasing as the specimen was weakening due to crack length growth.

Table 2. The pre-crack termination values and test conditions.

Pre-crack termination values	
Final crack length (a_p)	6 mm
Stress intensity range (ΔK)	11 MPa·m$^{0.5}$
Force ratio	0.1
Cycle waveform	Sinusoidal
FCGR test conditions	
Environment and relative humidity	Air, 35~60%
Temperature	20 ± 5 °C
Measurement interval of crack length (a)	0.25 mm
Force frequency	15
Force ratio	0.1
Waveform	Sinusoidal
Initial stress-intensity range (ΔK_i)	11 MPa·m$^{0.5}$
Force	2 kN

Fractographic analysis was carried out using a JEOL JS-6610 scanning electron microscope (SEM) (JEOL, Peabody, MA, USA), to evaluate the fracture surfaces of the FCGR specimens built through DMLS in Ti6Al4V(ELI). For each specimen built in the XZY, YXZ- and ZXY-orientations, the fracture surface characteristics were examined. The depth of field of the SEM enabled a detailed assessment of the various fracture modes resulting from the FCGR tests.

3 Results and discussion

3.1 Microstructure analysis

The microstructures of the Ti6Al4V(ELI) specimens produced through DMLS and subjected to the two-stage heat treatment are depicted in Figure 2. As-built Ti6Al4V(ELI) specimens were reported to have an α′-martensite microstructure [31]. These microstructures, after the two-stage heat treatment, were consistent across the FCGR specimens produced in the three orthogonal build planes, as shown in Figure 2. They reveal acicular α-phase, a small amount of β-phase, and evidence of partial α globulisation, as indicated by the arrows in Figure 2. Similar microstructures were reported in a previous study and were associated with DMLS Ti6Al4V(ELI) specimens exhibiting high tensile strength properties [2].

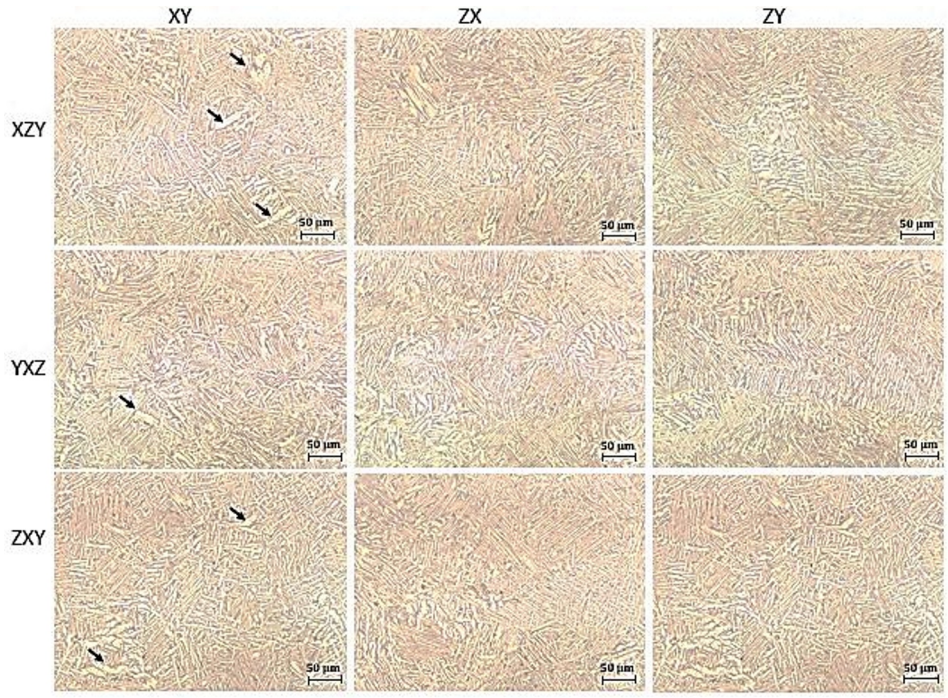

Fig. 2. Images of the microstructures obtained in the current study in XY-, ZX- and ZY-planes for specimens built in the XZY, YXZ and ZXY orientations from Ti6Al4V(ELI) through DMLS and followed by two-stage heat treatment.

3.2 Tensile properties of SLM Ti6Al4V(ELI)

In Table 3, the average tensile properties of the triplicate DMLS Ti6Al4V(ELI) specimens built along each of the X-, Y- and Z-orientations, and subsequently submitted to the two-stage heat treatment, are presented. The highest elastic modulus, yield strength and ultimate tensile strength were recorded on the specimens that were oriented along the X- and Y-axes, whereas the Y-orientation specimens had the lowest percentage elongation. These results are comparable to those found in a previous study on Ti6Al4V(ELI) specimens produced by DMLS and heat-treated similarly, but that were machined from bars to obtain the specified test specimen geometry [29].

Table 3. Average tensile properties of the Ti6Al4V(ELI) specimens built through DMLS, followed by two-stage heat treatment.

Specimen Orientations	Youngs's Modulus (GPa)	Yield Strength (σ_{ys}) (Offset 0.2%) (MPa)	UTS (MPa)	Elongation %
X	115	856	943	15
Y	117	860	944	14
Z	109	779	892	15
X [29]	120	846	933	15
Y [29]	120	851	931	18
Z [29]	108	765	910	14

The yield strengths of X and Y specimens were comparable after two-stage heat treatment, whereas the Z specimens recorded 10% less than that of the X and Y specimens. These results are comparable with the mechanical properties of wrought Ti6Al4V(ELI) [32]. Importantly, the lowest recorded yield strength, UTS and elongation shown in Table 3 are still comparable with the tensile properties of 780 MPa, 860 MPa and 15%, respectively, required in the aircraft industry [33].

3.3 FCGR of DMLS Ti6Al4V(ELI) specimens

The FCGR properties of triplicate Ti6Al4V(ELI) specimens, produced through DMLS in three orientations (XZY, YXZ and ZXY) and subsequently submitted to the two-stage heat treatment, are given in Table 4. ΔK_{th} is the fatigue crack growth threshold that signifies the critical value of ΔK below which crack growth will not occur.

Table 4. FCGR properties of the Ti6Al4V(ELI) specimens, built through DMLS and followed by two-stage heat treatment. SD = standard deviation.

Specimen orientations	ΔK_{th} ($1e^{-8}$) (MPa·$m^{0.5}$)	ΔK_{th} ($1e^{-7}$) (MPa·$m^{0.5}$)	Coefficients	
			C	m
XZY1	0.653	1.465	3.37	2.85
XZY2	0.661	1.477	3.328	2.86
XZY3	0.761	1.661	2.24	2.95
Mean	**0.692**	**1.534**	**2.963**	**2.89**
SD	**0.049**	**0.090**	**0.523**	**0.045**
YXZ1	0.569	1.288	4.98	2.76
YXZ2	0.463	1.111	7.64	2.65
YXZ3	0.504	1.183	6.36	2.70
Mean	**0.512**	**1.194**	**6.327**	**2.70**
SD	**0.044**	**0.073**	**1.086**	**0.045**
ZXY1	0.539	1.261	5.33	2.71
ZXY2	0.552	1.325	4.55	2.80

ZXY3	0.577	1.325	4.59	2.77
Mean	**0.556**	**1.304**	**4.823**	**2.76**
SD	**0.016**	**0.030**	**0.359**	**0.037**

The FCGR values of the Ti6Al4V(ELI) specimens produced by DMLS in various orientations in the current study depicted an improvement of this property as compared to the previous studies given, see Table 5. For example, the slope (m value) of the FCGR versus ΔK based on the current results is lower than the values reported in the previous studies for all specimen build orientations.

Table 5. FCGR values of Ti6Al4V(ELI) specimens built through DMLS and annealed at high temperature from different sources.

Built orientation	**LPBF technology**	**Annealing Temperature (°C)**	**ΔK_{th} ($MPa \cdot m^{0.5}$)**	**C**	**m**	**Source**
Wrought (Annealed Grade 5)	-	-	-	$1.85e^{-10}$	3.8	[6]
-	EOSINT M290 (DMLS)	913 for 3h and 1020 for 2h	-	$1.27e^{-10}$	3.5	
-		913 for 3h, followed by 1020 for 0.5h	-	$4.11e^{-1}0$	3.2	
-		913 for 3h and fluctuating between 875 to 975 for 24h	-	$3.81e^{-10}$	3.3	
∥ to deposition	EOSINT M280 (DMLS)	920 for 0.5h	8.0		3.9	[28]
⊥to deposition			8.1		3.5	
XZY	EOSINT M280 (DMLS)	910 for 8h	2.7	$1.87e^{-11}$	3.51	[34]
YXZ			3.5	$1.87e^{-11}$		
ZXY			2.7	$1.87e^{-11}$		
XZY	SLM	890 for 2h	-	$2.58e^{-11}$	2.94	[22]
YXZ				$2.04e^{-12}$	3.83	
ZXY				$1.71e^{-11}$	3.11	

In Figure 3, FCGR versus ΔK graphs obtained in the current study are shown. Clearly, the two-stage heat treatment performed in the current study improved the FCG resistance of the Ti6Al4V(ELI) produced through DMLS compared to the work presented in Table 5. This was done by altering the microstructure of the DMLS Ti6A4V(ELI) specimens from martensitic microstructure into lamellar α-phase, with a small amount of β-phase. Ti6Al4V(ELI) specimens built through DMLS, followed by a two-stage heat treatment, depicted a very slow crack growth during the initial stage of crack propagation. ΔK increased directly proportional to the crack length, leading to rapidly increasing crack propagation.

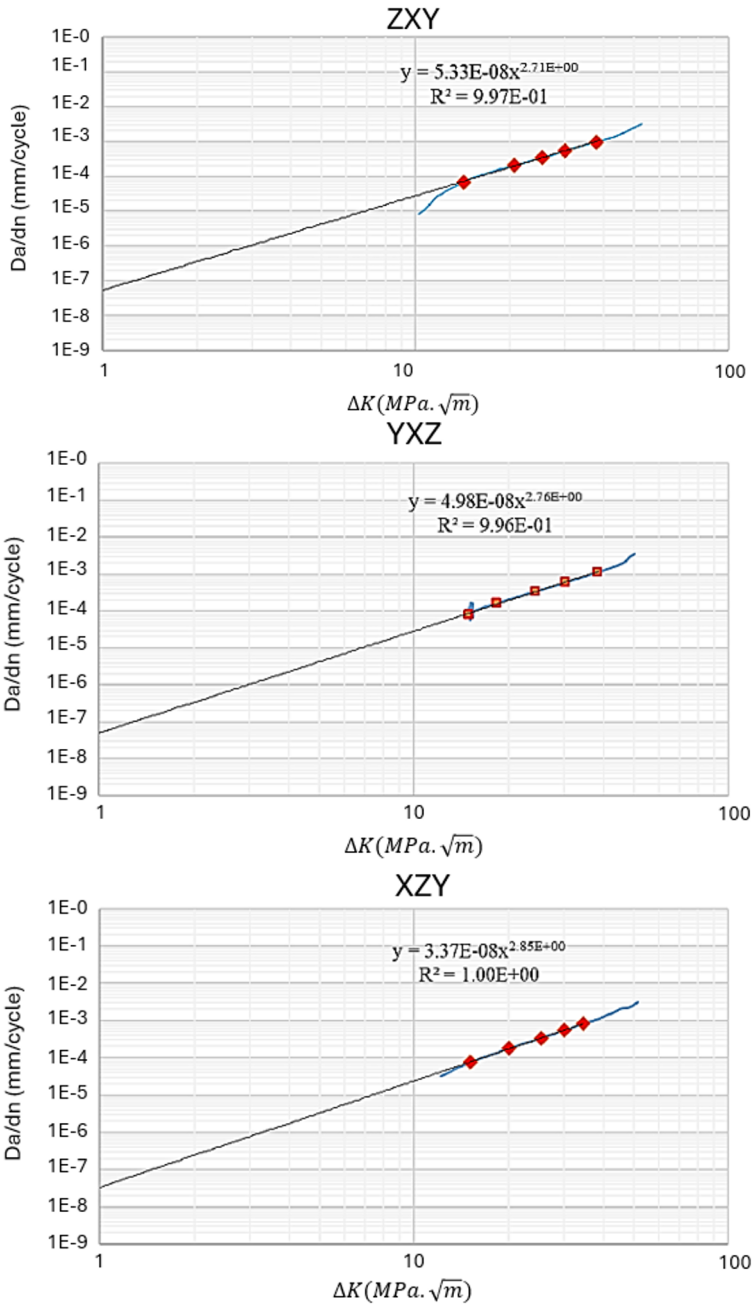

Fig. 3. FCGR versus stress intensity factor range plot for all Ti6Al4V(ELI) specimens built by DMLS in various orientations (XZY, YXZ, and ZXY), followed by two-stage heat treatment and the crack growth plot of the same specimens.

In a previous study, Syed et al. [5] reported that a stress relieving heat treatment reduced residual stress by 90%, resulting in reduced FCGR when compared to as-built DMLS Ti6Al4V(ELI) specimens. On the other hand, Beal et al. [6] demonstrated that high temperature annealing (HTA) resulted in a FCGR improvement of about 45%. Therefore, it can be concluded, that the HTA process is the major contributor to an improved FCGR.

The critical crack length was determined for the Ti6Al4V(ELI) specimens under cyclic load, as indicated in Figure 4.

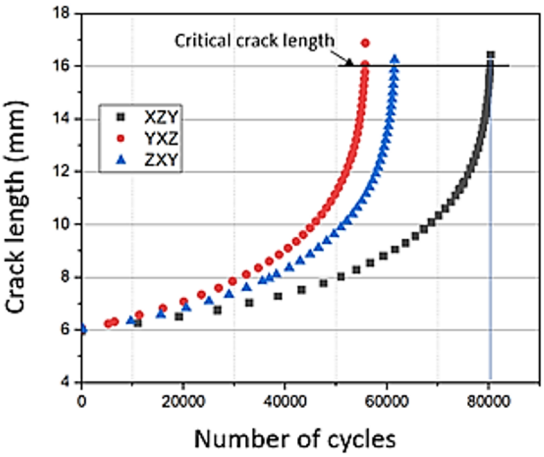

Fig. 4. The plot of crack length vs number of cycles to failure of the DMLS Ti6Al4V(ELI) specimens built in orientations (XZY, YXZ, and ZXY), followed by two-stage heat treatment.

The specimens in the YXZ orientation reached the critical crack length at the lowest number of cycles. In these specimens, the cracks propagated until they reached the critical size of about 16 mm after ~ 55 000 cycles, followed by final fracture, whereas specimens ZXY and XZY reached the critical size of 16 mm at 60 000 and 80 000 cycles, respectively.

3.4 Fractographic results

Figure 5 presents SEM images of the fracture surfaces of the Ti6Al4V(ELI) FCGR test specimens.

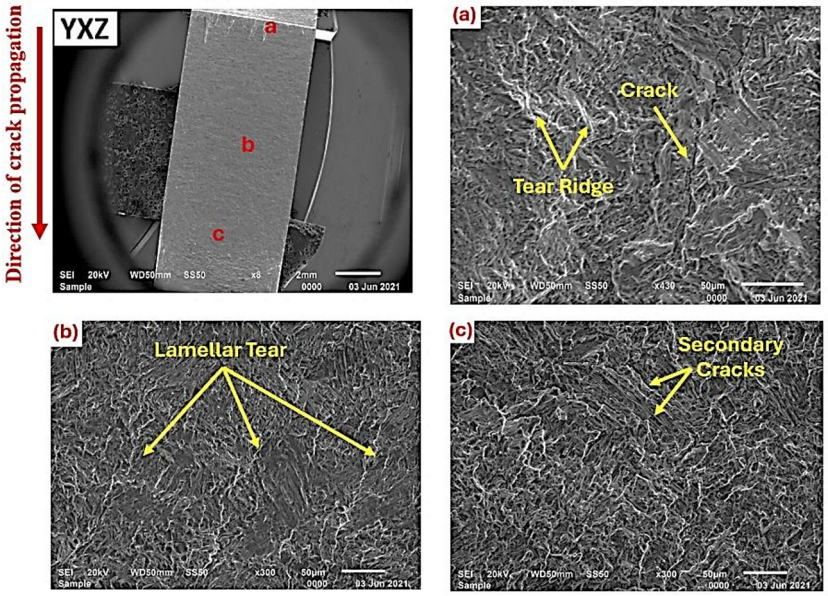

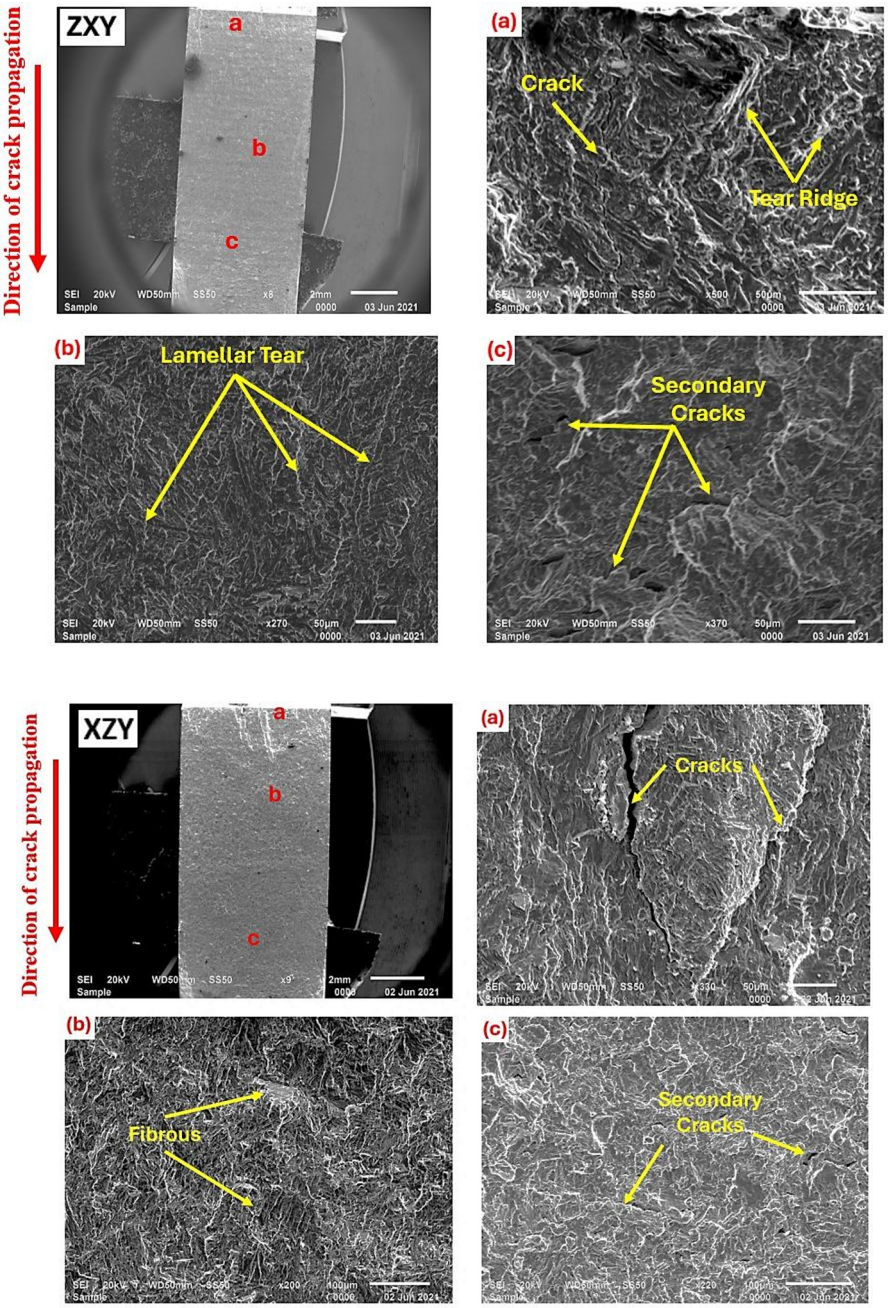

Fig. 5. Representative SEM images of the fracture surfaces of XZY, YXZ and ZXY specimens indicating the (a) crack initiation region, (b) crack propagation area and (c) final fracture region.

In all SEM images, the crack propagation direction is from the top to the bottom of the images, as illustrated by the red arrow. The crack initiation regions exhibited tear ridges forming river-like patterns. Dimples, along with some inter-lamellar tears, were observed in the crack propagation areas of the specimens. In the final fracture region, secondary cracks were present, oriented approximately perpendicular to the primary crack plane. Overall, the

fracture surfaces of all specimens displayed tortuous features, indicative of ductile metal and strong metallurgical bonds between the DMLS layers.

Crack initiation occurred at the notch-tip of the DMLS Ti6Al4V(ELI) FCGR specimens due to high stress concentration. The secondary crack size on the XZY specimen was found to be significantly larger than those shown by the YXZ and ZXY specimens, see Figure 5(a). This was attributed to the build orientation of the deposited layers, which was perpendicular to the direction of the applied load. Moreover, this large crack size is consistent with the lower UTS of Z specimens when compared to X and Y specimens. In the region of crack initiation, tear ridges were also present, suggesting that the DMLS Ti6Al4V(ELI) FCGR specimens experienced plastic deformation as the cracks grew. These demonstrated that the FCGR specimens had the required ductility that resulted from the two-stage heat treatment performed on all specimens.

In the crack propagation region shown in Figure 5(b), fibrous features were depicted in the XZY specimen, whereas specimens YXZ and ZXY displayed a lamellar tear fracture mode. These confirmed that the SLM Ti6Al4V(ELI) FCGR specimens had ductile properties. Final fracture occurred in all specimens, with secondary cracks suggesting that failure resulted from elastic stress concentration.

A flat face fracture feature was also depicted, as shown in the ZXY specimen in Figure 6. The flat faces were observed in the final fracture region. This confirmed that rapid crack growth across a crystallographic plane occurred in the ZXY DMLS Ti6Al4V(ELI) FCGR specimen.

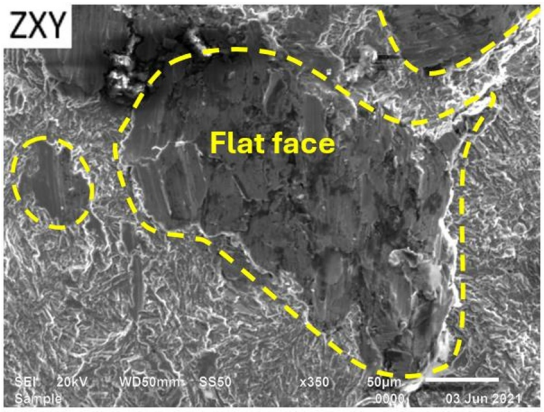

Fig. 6. SEM images showing a flat faced fracture feature in the ZXY specimen.

In general, the fractographic results corresponded with the microstructures consisting of acicular α and a small amount of β, with evidence of some α globulisation of the DMLS Ti6Al4V(ELI) FCGR specimens. These results also demonstrated a direct match with the tensile properties.

4 Conclusions

From the results obtained in this study, the following conclusions are drawn:

- The Ti6Al4V(ELI) specimens built through DMLS and followed by a two-stage heat treatment showed slightly anisotropic tensile properties, with the percentage difference between build orientations remaining below 10%. However, even the lowest tensile properties measured were comparable to those of the wrought

Ti6Al4V(ELI) alloy and met the aircraft industry's specifications, thereby confirming the high quality of the DMLS process.

- An improvement in the FCG resistance of the Ti6Al4V(ELI) specimens produced by DMLS was observed in this study compared to previous research, with the critical crack size determined to be 16 mm.
- The fractographic and metallographic results confirmed the tensile mechanical properties of the DMLS Ti6Al4V(ELI) FCGR specimens.
- The findings from this study highlight that, when properly controlled, DMLS processes can potentially be applied to produce mission-critical aircraft structural components in Ti6Al4V(ELI).

The authors express their gratitude to the South African Department of Science and Innovation through the Collaborative Program in Additive Manufacturing [Contract No.: CSIR-NLC-CPAM-21-MOA-CUT-01 and CPAM-25-IND-03] for the funding support. Moreover, the financial support from the Chair in Innovation and Commercialisation of Additive Manufacturing is also gratefully acknowledged. Research and development support of the Central University of Technology, Free State, through the emerging researcher programme, is also acknowledged.

References

1. R. Konečná, L. Kunz, A. Bača, G. Nicoletto, Long Fatigue Crack Growth in Ti6Al4V Produced by Direct Metal Laser Sintering. Procedia Eng. **160**, xviii, pp. 69–76, (2016). https://doi:10.1016/j.proeng.2016.08.864
2. T.H. Becker, M. Beck, C. Scheffer, Microstructure and mechanical properties of direct metal laser sintered TI-6AL-4V. South African J. Ind. Eng., **26**, p. 6, (2015). https://doi.org/10.7166/26-1-1022
3. J.P. Kruth, G. Levy, F. Klocke, T.H.C. Childs, Consolidation phenomena in laser and powder-bed based layered manufacturing. CIRP Ann. - Manuf. Technol., **56**, 2, pp. 730–759, (2007). https://doi:10.1016/j.cirp.2007.10.004
4. Z.A. Mierzejewska, R. Hudák, J. Sidun, Mechanical properties and microstructure of DMLS Ti6Al4V alloy dedicated to biomedical applications. Materials (Basel)., **12**, 1, pp. 1–17, (2019). https://doi:10.3390/ma12010176
5. A.K. Syed, B. Ahmad, H. Guo, T. Machry, D. Eatock, J. Meyer, M.E. Fitzpatick, X Zhang, An experimental study of residual stress and direction-dependence of fatigue crack growth behaviour in as-built and stress-relieved selective-laser-melted Ti6Al4V. Mater. Sci. Eng. A, **755**, pp. 246–257, (2019). https://doi:10.1016/j.msea.2019.04.023
6. R. Beal, S.D. Salehi, O.T. Kingstedt, Additively manufactured Ti-6Al-4V microstructure tailoring for improved fatigue life performance. Fatigue Fract. Eng. Mater. Struct. **47**, 7, pp. 2599–2615, (2024), https://doi:10.1111/ffe.14316
7. F.I. Jamhari, F.M. Foudzi, M.A. Buhairi, A.B. Sulong, N.A.M. Radzuan, N. Muhamad, I.F. Mohamed, N.H. Jamadon, K.S. Tan, Influence of heat treatment parameters on microstructure and mechanical performance of titanium alloy in LPBF: A brief review. J. Mater. Res. Technol. **24**, pp. 4091–4110, (2023). https://doi:10.1016/j.jmrt.2023.04.090
8. L.F. Monaheng, W.B. Preez, N. Kotze, M. Vermeulen, Topology optimisation of an aircraft nose-wheel fork for production in Ti6Al4V by the Aeroswift high-speed laser powder bed fusion machine. 14th World Conf. Titan. **321**, MATEC Web Conf, pp. 1–11, (2020). https://doi.org/10.1051/matecconf/202032103013

9. M. Khorasani, A.H. Ghasemi, B. Rolfe, I. Gibson, Additive manufacturing a powerful tool for the aerospace industry. Rapid Prototyp. J. (2021). https://doi:10.1108/RPJ-01-2021-0009
10. S. Singamneni, Y. LV, A. Hewitt, R. Chalk, W. Thomas, D. Jordison, Additive manufacturing for the aircraft industry: A review. J. Aeronaut. Aerosp. Eng. **08**, 01, (2019). https://doi:10.35248/2168-9792.19.8.215
11. H. Gong, K. Ra, H. Gu, G.D.J. Ram, T. Starr, B. Stucker, Influence of defects on mechanical properties of Ti6Al4V components produced by selective laser melting and electron beam melting, Mater. Des. **86**, pp. 545–554, (2015). https://doi:10.1016/j.matdes.2015.07.147
12. A.A.A. Aliyu, C. Puncreobutr, J Shinjo, S. Kuimalee, T. Phetrattanarangsi, T. Boonchuduang, P. Taweekitikul, C. Panwisawas, W Li, K. Poungsiri, B. Lohwongwatana, Lack of fusion-induced cracking effect on tensile and fatigue behaviours of laser powder-bed fusion-processed Ti-6Al-4V implant. Eng. Fail. Anal. **168**, p. 109095, (2025). https://doi:10.1016/j.engfailanal.2024.109095
13. L.F. Monaheng, W.B. Du Preez, C. Polese, Failure analysis of a landing gear nose wheel fork produced in Ti6Al4V(ELI) through selective laser melting. Eng. Fail. Anal. p., 107548, (2023), https://doi.10.1016/j.engfailanal.2023.107548
14. C. Dordlofva, P. Törlind, Qualification challenges with additive manufacturing in space applications. Solid Freeform Fabrication, pp. 2699–2712, (2017).
15. L. Portolés, O. Jordá, L. Jordá, A. Uriondo, M. Esperon-Miguez, S. Perinpanayagam, A qualification procedure to manufacture and repair aerospace parts with electron beam melting. J. Manuf. Syst. **41**, pp. 65–75, (2016). https://doi:10.1016/j.jmsy.2016.07.002
16. D.W. Gibbons, J.P.L. Serfontein, A.F. van der Merwe, Mapping the path to certification of metal laser powder bed fusion for aerospace applications. Rapid Prototyp. J. **27**, 2, pp. 355–361, (2021). https://doi:10.1108/RPJ-07-2020-0154
17. Federal Aviation Administration, Part 23 of CASR Airworthiness standards for aeroplanes in the normal, utility, acrobatic or commuter category, (2010). https://www.casa.gov.au/search-centre/rules/part-23-casr-airworthiness-standards-aeroplanes-normal-utility-acrobatic-or-commuter-category
18. SACAA, South African Civil Aviation Technical Standards 21, (2012). https://www.gov.za/sites/default/files/gcis_document/202111/45491rg11359gon1503.pdf
19. EASA, Certification Specifications and Acceptable Means of Compliance for Large Aeroplanes. European Union Aviation Safety Agency. (2012). https://www.easa.europa.eu/certification-specifications/cs-25-large-aeroplanes
20. ASTM International, Standard Test Method for Measurement of Fatigue Crack Growth Rates, (2016). https://doi:10.1520/E0647-15E01.2
21. S.L.G. Assias, H.G. Kotik, J.E.P. Ipiña, Fracture surface analysis of fracture mechanics specimens with splits: Determination of the physical crack extension. Theor. Appl. Fract. Mech. **133**, p. 104509, (2024). https://doi:10.1016/j.tafmec.2024.104509
22. V.E.M. Cain, L. Thijs, J. Van Humbeeck, B. Van Hooreweder, R. Knutsen, Crack propagation and fracture toughness of Ti6Al4V alloy produced by selective laser melting. Addit. Manuf. **5**, pp. 68–76, 2015, https://doi:10.1016/j.addma.2014.12.006
23. D. de Beer, W.B. du Preez, H. Greyling, F. Prinsloo, F. Sciammarella, N. Trollip, M. Vermeulen, T. Wohlers, A south african additive manufacturing strategy. Dep. Sci. Technol. pp. 1–92, (2016).

24. ASTM International, ASTM E8/E8M standard test methods for tension testing of metallic materials. (2010). https://doi:10.1520/E0008
25. ASTM International, ASTM E647−23a, Standard Test Method for Measurement of Fatigue Crack Growth Rates, Am. Soc. Test. Mater. pp. 1–50, (2014), https://doi:10.1520/E0647-23A.2
26. ASTM International, Standard Specification for Additive Manufacturing Titanium-6 Aluminum-4 Vanadium ELI (Extra Low Interstitial) with Powder Bed Fusion. Int. ASTM, (2014). https://doi:10.1520/F3001-14
27. L.F. Monaheng, W.B. du Preez, C. Polese, Towards Qualification in the Aviation Industry: Impact toughness of Ti6Al4V(ELI) specimens produced through laser powder bed fusion followed by two-stage heat treatment, Metals (Basel). **11**, 1736, pp. 1–12, (2021), https://doi.org/10.3390/met11111736
28. P. Kumar, U. Ramamurty, Microstructural optimization through heat treatment for enhancing the fracture toughness and fatigue crack growth resistance of selective laser melted Ti6Al4V alloy. Acta Mater. **169**, pp. 45–59, (2019), https://doi:10.1016/j.actamat.2019.03.003
29. L.B. Malefane, W.B. du Preez, M. Maringa, A. du Plessis, Tensile and high cycle fatigue properties of annealed TI6AL4V (ELI) specimens produced by direct metal laser sintering, South African J. Ind. Eng. **29**, 3 Special Edition, pp. 299–311, (2018). https://doi:10.7166/29-3-2077
30. T.L. Anderson, Fracture Mechanics: Fundamentals and Applications, Third Edition. (2005). https://doi:10.1002/1521-3773(20010316)40:6<9823::AIDANIE9823>3.3.CO;2-C .
31. B. Vrancken, L. Thijs, J.P. Kruth, J. Van Humbeeck, Heat treatment of Ti6Al4V produced by selective laser melting: Microstructure and mechanical properties, J. Alloys Compd. **541**, pp. 177–185, (2012), https://doi:10.1016/j.jallcom.2012.07.022
32. AZoM, Grade 23 Ti 6Al 4V ELI Alloy (UNS R56401), (2013). https://www.azom.com/article.aspx?ArticleID=9365
33. ASM Aerospace Specification Metals Inc, Titanium Ti-6Al-4V (Grade 5), ELI, Annealed. Jun. 29, (2021). http://asm.matweb.com/search/SpecificMaterial.asp?bassnum=MTP643
34. N. Macallister, K. Vanmeensel, T. Hermann, Fatigue crack growth parameters of Laser Powder Bed Fusion produced Ti6A4V, Int. J. Fatigue, **145**, p. 106100, (2021). https://doi:10.1016/j.ijfatigue.2020.106100.